

Rainfall Infiltration and Slope Stability: a case study in Marumori, Miyagi, Japan

Nilo Lemuel J. DOLOJAN, Department of Civil Engineering, Tohoku University
 Shuji MORIGUCHI, IRIDeS, Tohoku University
 Kenjiro TERADA, IRIDeS, Tohoku University
 FAX +81-22-752-2133, E-mail: dolojan.nilo.lemuel.junior.r2@dc.tohoku.ac.jp

Shallow landslides and slope failures in Marumori, Miyagi during the October 2019 typhoon Hagibis are acknowledged to be induced by heavy rainfall. Using rainfall intensity and soil characteristics, infiltration capacity and depth of infiltration can be estimated. In this study, the Green-Ampt equation, adapted for inclined surfaces, is used to estimate infiltration depths along critical slopes. Assigning the computed infiltration depths as the slip surface depth, the factor of safety is then calculated using the infinite slope stability model. Translating this model into raster processes, a visualization map of a time-varying factor of safety for Marumori can be generated.

1. Introduction

Rainfall is one of the most common triggers for landslides. This study aims to determine the relationship of rainfall with slope instability using simplified rainfall infiltration and slope stability models. The study also intends to estimate time of occurrence of slope failure, which may be extended to future slope failures through rainfall forecasts. For this purpose, the Green-Ampt infiltration equation and the infinite slope stability model were utilized in the conduct of the research.

2. Green-Ampt Infiltration Equation

Green and Ampt¹⁾ proposed a one-dimensional analytical solution for rainfall infiltration where an excess of water at the ground surface, or ponding, is present. Under constant rainfall and ponding conditions, the model assumes infiltration through homogenous soil with uniform initial water content and constant soil suction head at the wetting front. Moreover, it assumes water penetration characterized by a sharp wetting front which separates the soil at maximum saturation from the soil at initial moisture. To extend the applicability of the Green-Ampt model for time-varying rainfall, Chu²⁾ modified the equations into:

$$F(t)_{t+\Delta t} = F(t) + K\Delta t + \psi\Delta\theta \ln\left(\frac{F_{t+\Delta t} + \psi\Delta\theta}{F(t) + \psi\Delta\theta}\right) \quad (1)$$

$$f(t)_{t+\Delta t} = K\left(\frac{\psi\Delta\theta}{F(t)_{t+\Delta t}} + 1\right) \quad (2)$$

$$F(t)_p = \frac{K\psi\Delta\theta}{i_t - K} \quad (3)$$

where $F(t)$ is the cumulative infiltration at time t , $f(t)$ is the infiltration rate at time t , $F(t)_p$ is the cumulative infiltration at ponding time, and i_t is the rainfall intensity at time t . The input parameters are hydraulic conductivity K , wetting front soil suction head (capillary head) ψ , change in volumetric water content $\Delta\theta$, and rainfall intensity i . However, these equations only considered infiltration and ponding along level horizontal surfaces. To address this issue, Chen³⁾ further modified the equations to adapt the model for inclined surfaces. Using the slope angle α , the cumulative infiltration, infiltration rate, and ponding cumulative infiltration measured normal to the inclined sloping surface can be rewritten as:

$$F(t)_{t+\Delta t} = F(t) + K\cos\alpha\Delta t + \frac{\psi\Delta\theta}{\cos\alpha} \ln\left(\frac{F_{t+\Delta t}\cos\alpha + \psi\Delta\theta}{F(t)\cos\alpha + \psi\Delta\theta}\right) \quad (4)$$

$$f(t)_{t+\Delta t} = K\left(\frac{\psi\Delta\theta}{F(t)_{t+\Delta t}} + \cos\alpha\right) \quad (5)$$

$$F(t)_p = \frac{K\psi\Delta\theta}{i_t - K\cos\alpha} \quad (6)$$

During a rainfall event, the mechanism of infiltration may coincide into three possible scenarios shown in Fig.1. These are:

- 1) Potential infiltration rate $f(t)$ is greater than rainfall intensity. All rainfall can be accommodated by the soil, hence there is no ponding, and $F(t)$ is equivalent to the cumulative rainfall.
- 2) Potential infiltration rate is greater than the rainfall intensity at the beginning of the time interval, but becomes less than the latter towards the end. Ponding occurs within the interval. $F(t)$ is calculated from Equation (6).
- 3) Potential infiltration rate is less than or equal to the rainfall intensity. Not all rainfall can enter the soil, ponding and runoff occurs throughout the time interval. $F(t)$ is calculated using Equation (4).

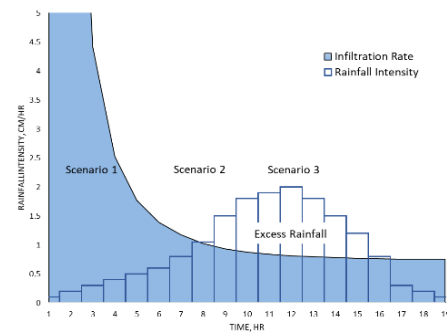


Fig. 1 Infiltration Rate and Rainfall Intensity

From the cumulative infiltration, the depth of the wetting front z , measured from the vertical can be calculated as:

$$z = \frac{F(t)}{\Delta\theta\cos\alpha} \quad (7)$$

3. Infinite Slope Stability Model

Like most slope stability equations, the factor of safety in an infinite slope model is the ratio between the resisting force and the driving force. For an infinite slope, the shear strength is based on the Mohr-Coulomb failure criterion, while the shear stress is the force in the tangential direction due the weight of the soil:

$$FS = \frac{c' + (\sigma_n - u) \tan\phi'}{\sigma_t} \quad (8)$$

where τ is the shear strength, c' is the effective cohesion, ϕ' is the effective angle of internal friction, $(\sigma_n - u)$ is the effective normal stress with σ_n being the normal stress on the slip surface and u being the pore pressure, and σ_t is the shear stress or the tangential component of the weight of the soil.

However, for shallow slope failures, pore pressures attributed to full saturation caused by rise of groundwater level is absent and the depth of slip surface is represented as the depth of wetting

front. Substituting the unit weight of the soil γ and the depth of wetting front z into the gravitational weight of the soil; and getting their normal and tangential components, the stability model can be simplified into:

$$FS = \frac{c' + z\gamma_{soil}\cos^2\alpha \tan\phi'}{z\gamma_{soil}\sin\alpha \cos\alpha} \quad (9)$$

4. Case Study

For this study, the terrain and soil characteristics of Marumori, Miyagi were considered. The rainfall data used in this study shown in Fig.2 was from 11 Oct 2019 23:00 to 13 Oct 2019 03:00, spanning 29 hours, during Typhoon 19 as recorded from the Marumori Weather Station⁴⁾. Soil types and bulk densities of Marumori were derived from soilgrids.org⁵⁾. The Green-Ampt Parameters⁶⁾ for Loam, the most dominant soil type in Marumori, are $K=0.66$ cm/hr, $\psi=8.89$ cm, $\Delta\theta=$ (total porosity - field capacity) $=0.193$. The angle of internal friction⁷⁾ used was $\phi'=28.1^\circ$, while the unit weight was derived from the bulk density. In the interest of analyzing the worst-case scenario, a cohesion of $c'=1kPa$ was assumed.

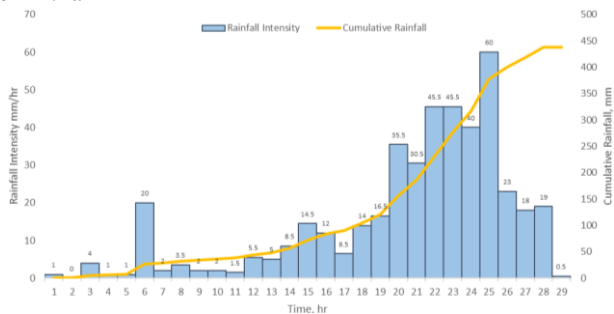


Fig. 2 Rainfall data

5. Results

The simulations were run in a 2373x2249 grid with slope and elevation data of 10m resolution. 250 m resolution soil type and bulk density data were resampled as 10 m for data interoperability. The equations were run iteratively into each cell resulting into 29 time-series raster grids. Of these results, representative cells with angles: 35°, 45°, 55°, 65°, 75°, were selected and are shown in Fig. 3.

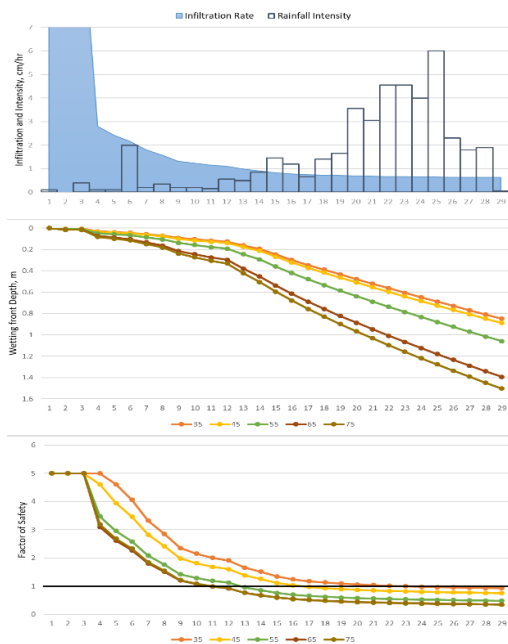


Fig. 3 Infiltration rate, wetting front depth, and factor of safety through time

The results show that as the slope angle increases, the change in both the wetting front depth and the factor of safety increases significantly. It is also shown that steeper slopes reach a state of failure ($FS < 1.0$) earlier than gentler ones. Particularly, slopes with angle 75°, 65°, 55°, 45°, and 35° become unstable at time 11, 11, 13, 17, and 23 respectively.

Figure 4 shows a map of decreasing factors of safety within Marumori on different time intervals. The factor of safety is represented as deep red: <0.5 ; red: $0.5-0.75$; orange: $0.75-1.0$; yellow: $1.0-1.25$.

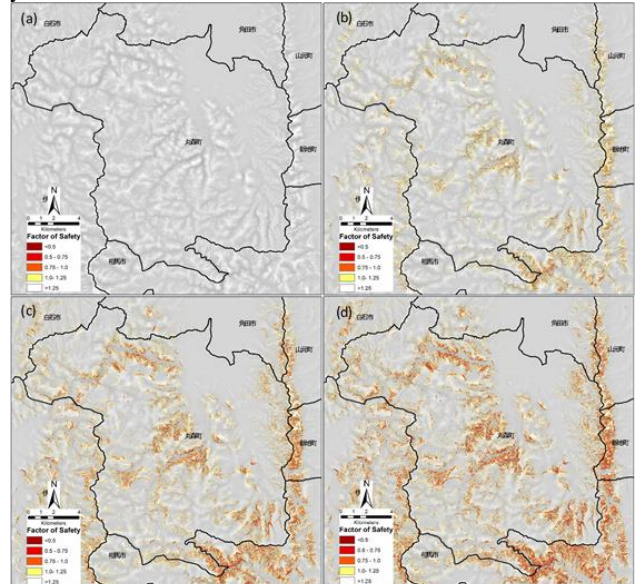


Fig. 4 Computed factor of safety at time (a) $t=1$, 11 Oct 2019 23:00; (b) $t=17$, 12 Oct 2019 15:00; (c) $t=23$, 12 Oct 2019 20:00; (d) $t=29$, 13 Oct 2019 03:00

Initially, the soil has not been saturated and all slopes are stable with $FS > 1.25$ (Fig.4a). At time=17, the wetting front has advanced as much as 0.95m, and most slopes $>40^\circ$ have become unstable (Fig.4b). Also, marginally stable slopes ($FS=1-1.25$) were measured to have inclinations of mostly 30° to 40° (measured 1 std. dev from the mean). At time=23 (Fig.4c), the furthest wetting front has advanced 1.42m, and majority of the slopes steeper than 35° have become unstable. At this time, slopes ranging from 26° to 35° are reduced to marginally stable conditions. By time=29 (Fig.4d), the wetting front has gone 1.81m into the surface. Slopes inclined 30° to 40° now comprise majority of the unstable slopes, and slopes ranging from 24° to 34° are now reduced to marginally stable conditions.

In conclusion, a visual representation of the overall decline in stability is generated. Using rainfall forecast as input, the model may be extended as an early warning system during heavy rainfall.

References

- 1) W. H. Green and G. A. Ampt: Studies on Soil Physics, The Journal of Agricultural Science, 1911
- 2) S. T. Chu, Infiltration During an Unsteady Rain, Water Resources Research, 14, 1978.
- 3) L. Chen, M. H. Young: Green-Ampt infiltration model for sloping surface, Water Resources Research, 42, 2006.
- 4) Japan Meteorological Agency: AMeDAS, <http://www.data.jma.go.jp/obd/stats/etrn/index.php>, accessed 11 Dec 2019.
- 5) International Soil Reference and Information Centre, World Soil Information: Soil Grids, <https://soilgrids.org/>, accessed 17 Dec 2019.
- 6) D. R. Maidment: Handbook on Hydrology, McGraw-Hill, 1993.
- 7) Bureau of Reclamation: Earth manual 3rd Ed., U.S. Department of Interior, 1998.